# Substituent Effects on the Electronic Spectroscopy of Four-Carbon Criegee Intermediates

Tianlin Liu<sup>†</sup>, Meijun Zou<sup>†</sup>, Adriana Caracciolo<sup>‡</sup>, Christopher A. Sojdak, and Marsha I. Lester\* Department of Chemistry, University of Pennsylvania, Philadelphia, PA 19104-6323 USA

### **Abstract**

Atmospheric ozonolysis of biogenic and anthropogenic alkenes generates zwitterionic carbonyl oxide intermediates ( $R_1R_2C=O^+O^-$ ), known as Criegee intermediates, with different structural motifs and conformations. This study reports a systematic laboratory study of substituent effects on the electronic spectroscopy of four-carbon Criegee intermediates (CIs) with methyl-ethyl (MECI) and isopropyl (IPCI) groups, which are isomers produced in ozonolysis of asymmetric branched alkenes. The four-carbon CIs are separately generated by an alternative synthetic route and spectroscopically characterized on the strong  $\pi^* \leftarrow \pi$  transition associated with the carbonyl oxide group in a pulsed supersonic expansion with VUV photoionization at 118 nm and UV-induced depletion of the m/z 88 signal. The resultant broad and unstructured UV spectral features for MECI and IPCI are peaked at ca. 320 and 330 nm, respectively, with large absorption cross sections of ca. 10<sup>-17</sup> cm<sup>2</sup>. Comparisons are made with the four-carbon CIs formed in isoprene ozonolysis, methyl vinyl ketone oxide (MVK-oxide) and methacrolein oxide (MACRoxide), which have the same backbone connectivity as MECI and IPCI, but have extended conjugation across the vinyl and carbonyl groups. A remarkable 50 nm shift of the peak absorption to longer wavelength is observed for MVK-oxide and MACR-oxide compared to MECI and IPCI, respectively. Vertical excitation energies computed theoretically agree well with the experimental findings, confirming that the spectral shifts are caused by the extended  $\pi$  conjugation in the isoprene-derived Criegee intermediates.

<sup>\*</sup> Corresponding author email: milester@sas.upenn.edu

#### Introduction

Atmospheric ozonolysis of alkenes generates zwitterionic carbonyl oxide intermediates  $(R_1R_2C=O^+O^-)$ , known as Criegee intermediates (CIs). Since the size and structure of alkenes from anthropogenic and biogenic sources vary widely, ranging from ethene to large terpenes. CIs with different structural motifs and conformations are formed. Here, we examine substituent effects, specifically the influence of extended conjugation, on the electronic spectroscopy of four-carbon CIs generated in the laboratory. This study characterizes the methyl-ethyl substituted CI [(CH<sub>3</sub>CH<sub>2</sub>)(CH<sub>3</sub>)COO, MECI] and isopropyl substituted CI [(CH<sub>3</sub>)<sub>2</sub>(H)COO, IPCI], typically generated in ozonolysis of asymmetric branched alkenes, and compares their properties with methyl vinyl ketone oxide [(CH<sub>2</sub>=CH)(CH<sub>3</sub>)COO), MVK-oxide]<sup>2,3</sup> and methacrolein oxide [(CH<sub>2</sub>=C(CH<sub>3</sub>))CHOO, MACR-oxide]<sup>4</sup> formed in isoprene ozonolysis. MECI and IPCI have analogous backbone connectivity as MVK-oxide and MACR-oxide, respectively, but contain a saturated carbon chain and lack the resonance stabilization afforded by extended conjugation across the vinyl (C=C) and carbonyl oxide (C= $O^+O^-$ ) groups in the isoprene-derived CIs. MECI and IPCI are isomers, as are MVK-oxide and MACR-oxide, in both cases with structures differing only by the position of a methyl group. The structural similarities of these CIs are illustrated in Scheme 1, although we note that each CI has four low energy conformational forms as detailed below.

**Scheme 1**. Chemical structures of four structurally similar Criegee intermediates, noting that each CI has four low energy conformers.

MECI has two groups of conformational forms that differ in the orientation of the carbonyl oxide group, which may be oriented either towards the methyl (*anti*, *E*) or the ethyl (*syn*, *Z*) substituent as shown in Figure 1. The *anti* and *syn* conformers are separated by significant barriers (~37 kcal mol<sup>-1</sup>)<sup>5</sup> associated with internal rotation about the C=O bond. In each case, the ethyl substituent has two orientations that differ by internal rotation about a C-C bond, leading to a theoretical prediction of four minimum energy configurations with similar ground state energies (within 1 kcal mol<sup>-1</sup>).<sup>6</sup> MECI was initially observed and structurally characterized by Fourier transform microwave spectroscopy (FTMW) using jet-cooled conditions, following production in pulsed electric discharge of a 2,2-diiodobutane precursor and O<sub>2</sub>, where the four conformational forms were observed with similar relative abundances.<sup>6</sup> The four conformations of MECI are shown in Figure 1.

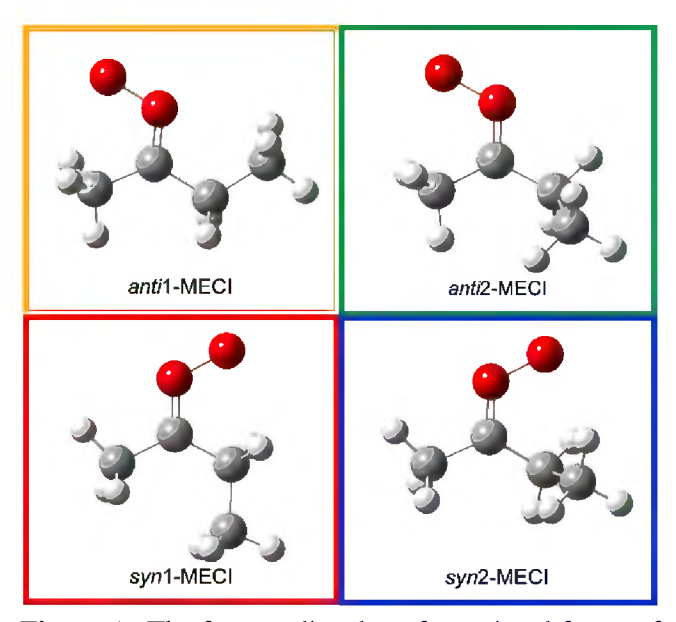


**Figure 1**. The four predicted conformational forms of the methyl-ethyl substituted Criegee intermediate (MECI). The *anti*1 and *syn*1 conformers are found to have  $C_s$  symmetry, while *anti*2 and *syn*2 conformers have  $C_1$  symmetry.

MECI has also been previously investigated by IR action spectroscopy in the CH overtone region  $(2v_{CH})^{.7}$  1,4 H-atom transfer and unimolecular decay yielded energy-dependent rates k(E) to OH radical products that were detected. Master equation modeling was utilized to extend the results to thermal unimolecular decay rates k(T) for *anti*- and *syn*-MECI, yielding 473 s<sup>-1</sup> (*anti*) and 660 s<sup>-1</sup> (*syn*), respectively, at 298 K (1 atm).

The structures and relative stabilities of four possible IPCI conformers have previously been characterized in an analogous FTMW and computational study. Again, the syn(Z) and anti(E) conformers are separated by significant barriers associated with internal rotation about the C=O bond, while relatively low barriers are predicted for internal rotation about the OCCC dihedral angles that separate the pairs of syn and anti conformers. In this case, theoretical prediction yielded lower energy syn conformers and higher energy anti conformers with ground state energies spread over ca. 3.7 kcal mol<sup>-1</sup>. Intramolecular hydrogen bonding between one or both methyl groups and the terminal oxygen in syn conformers of IPCI contributes to the greater stability of these conformers. Only two conformers, syn2 and anti1, were observed in Ar carrier gas (syn2:anti1 = 2.5:1), while three conformers, syn2, anti1, and anti2, were identified in Ne carrier gas (syn2:anti1:anti2 = 3.9:1.0:0.6), in both cases following production in pulsed electric discharge of 1,1-diiodo-2 methyl propane precursor and  $O_2$ . The lowest energy syn2 conformer is stabilized by a hydrogen-bonding interaction between a methyl group and terminal O-atom of the carbonyl oxide. The four predicted conformers of IPCI are shown in Figure 2.

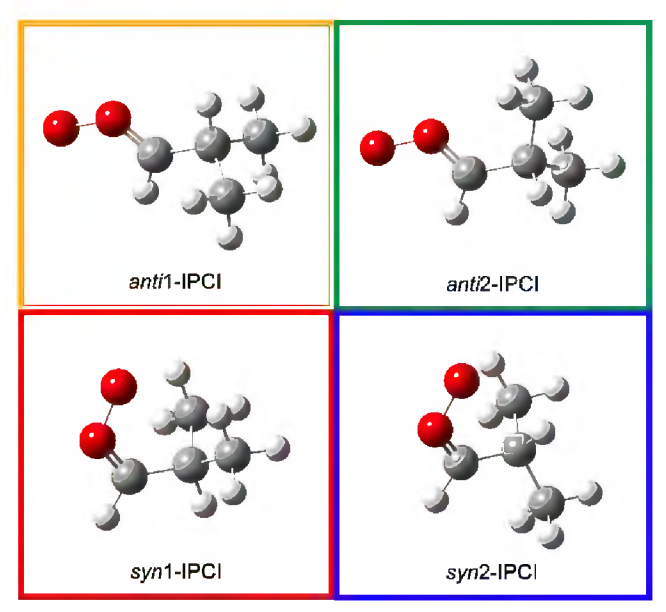


**Figure 2**. The four predicted conformational forms of the isopropyl-substituted Criegee intermediate (IPCI) with optimized geometries at the B2PLYP-D3/cc-pVTZ level of theory. The *anti*1 and *syn*1 conformers are found to have  $C_s$  symmetry, while *anti*2 and *syn*2 conformers have  $C_1$  symmetry.

This study examines the electronic spectroscopy of MECI and IPCI for the first time. Criegee intermediates have  $4\pi$  electrons associated with the zwitterionic carbonyl oxide group, giving rise to very strong  $\pi^* \leftarrow \pi$  electronic transitions and providing a sensitive way for detection of CIs. The MECI and IPCI spectroscopic results are compared with one another and then contrasted with the electronic spectra of isoprene-derived CIs, MVK-oxide<sup>3</sup> and MACR-oxide,<sup>4</sup> which are structurally similar four-carbon CIs but differ in having extended conjugation across the carbonyl oxide and vinyl groups.

# **Experimental and Theoretical Methods**

The methyl ethyl- and isopropyl-substituted Criegee intermediates (MECI and IPCI) are generated from 2,2-diiodobutane and 1,1-diiodo-2 methyl propane precursors, respectively. A detailed description of the synthesis of the 2,2-diiodobutane precursor has been reported previously.<sup>7</sup> A similar synthetic approach is used to produce the 1,1-diiodo-2 methyl propane precursor, differing in the starting material and final purification step. The synthetic procedures are detailed in supplementary information (SI).

Separate experimental studies are conducted on MECI and IPCI using analogous procedures. In both types of experiments, the diiodo alkane precursor is heated (45 °C for MECI and 60 °C for IPCI), entrained in a 20% Ar/O<sub>2</sub> carrier gas (10 psi), and pulsed through a solenoid valve (Parker-Hannifin General Valve Series 9) into a quartz capillary tube reactor (~25 mm length; 1 mm inner diameter). A Peltier thermoelectric heating module (Laird Technologies, PC4) is utilized with the temperature monitored by a thermocouple (Cole-Parmer, Type K digital thermometer). The precursor is photolyzed

by the 248 nm output (ca. 30 mJ/pulse) of a KrF excimer laser (Coherent COMPex 102), which is cylindrically focused along the capillary. The resultant monoiodo radicals from C-I bond breakage subsequently react with O<sub>2</sub> to form the Criegee intermediates. The Criegee intermediates are collisionally stabilized in the capillary and cooled in the ensuing supersonic expansion.

Approximately ~5 cm downstream, the gas mixture enters the interaction region of a time-of-flight mass spectrometer (TOF-MS), where the Criegee intermediates are photoionized using 118 nm (10.5 eV) VUV radiation and detected on the m/z=88 mass channel. The 118 nm VUV radiation is generated by frequency-tripling the third harmonic output (~32 mJ/pulse) of a Nd:YAG laser (Continuum Powerlite 9000, 4 ns) in a phase matched Ar/Xe gas mixture. UV radiation (290-380 nm, ≤ 4.5 mJ/pulse) is provided by the sum frequency or second harmonic output (OPO signal + 1064 nm Nd:YAG fundamental or second harmonic of OPO signal) of a broadly tunable β-barium borate optical parametric oscillator (BBO-OPO) source (EKSPLA 342NT, pulse width 3-5 ns, <5 cm<sup>-1</sup> linewidth), which is introduced ~ 50 ns prior to VUV photoionization detection. The focused UV beam (40 cm focal length) and VUV beam are counterpropagating and spatially overlapped in the interaction region.

Complementary theoretical studies were conducted for MECI and IPCI utilizing analogous methods as in prior studies.<sup>3, 4</sup> Ground state optimizations, anharmonic frequency calculations, and ionization energies were carried out for the four conformers of MECI and IPCI using the B2PLYP-D3/cc-pVTZ method and basis as implemented in Gaussian 16.<sup>9</sup> The optimized structures found for the four conformers of MECI and IPCI are shown in Figures 1 and 2. The relative (zero-point corrected) energies for the MECI and IPCI conformers are similar to prior reports,<sup>6-8</sup> and summarized in Tables S1-S2. The vertical and adiabatic ionization energies for the four conformers of MECI and IPCI are computed using the same method and basis.

The electronic vertical excitation energies (VEE) and corresponding oscillator strengths (f) for the lowest four singlet electronic transitions were calculated using the Complete Active Space with Second Order Perturbation Theory (CASPT2) with Dunning's augmented double- $\zeta$  basis set, aug-cc-pVDZ, assigned to all atoms. The CASPT2 calculations are based on a five-singlet state-averaged Complete Active Space-Self Consistent Field (SA5-CASSCF) reference wavefunction, involving an active space of 12 electrons in 10 orbitals. The 6 occupied orbitals encompass two  $\pi$  orbitals on the carbonyl oxide moiety, three  $\sigma$  orbitals across the whole molecule, and one 2p lone pair orbital localized on the oxygen atoms, while the 4 virtual orbitals include one  $\pi^*$  orbital and one  $\sigma^*$  orbitals localized on the carbonyl oxide group, one 3s Rydberg orbital and one 3p Rydberg orbital. A complete set of orbitals for the lowest energy conformers of MECI and IPCI are provided in SI (Figure S3). An imaginary level shift of 0.2  $E_H$  is employed in all CASPT2 calculations to mitigate effects of intruder states. Oscillator strengths for the

four vertical transitions (i=1-4) are evaluated using the CASSCF transition dipole moments ( $\mu_{0i}$ ) and CASPT2 vertical excitation energies ( $E_{0i}$ ) as follows:

$$f = \frac{2}{3} E_{0i} \sum_{\alpha = x, y, z} |\mu_{0i}|_{\alpha}^{2}$$

The energy required for spin-allowed dissociation of the lowest energy conformers of MECI and IPCI are evaluated using the same multireference methods. The product asymptotes are determined by relaxed optimization at large O-O separation leading to O (¹D) + butanone [CH<sub>3</sub>C(O)CH<sub>2</sub>CH<sub>3</sub>, X ¹A'] products for MECI and O (¹D) + isopropylaldehyde [(CH<sub>3</sub>)<sub>2</sub>CHCHO, X ¹A] products for IPCI. Zero-point energy corrections are obtained from B2PLYP-D3/cc-pVTZ calculations. The CASSCF and CASPT2 calculations were performed using the Molpro package. ¹0-12

#### **Results and Discussion**

The methyl-ethyl- and isopropyl-substituted Criegee intermediates are separately investigated, although the results are combined here. Each CI is initially detected by photoionization using 10.5 eV (118 nm) VUV radiation on its parent mass channel (m/z 88) in a TOF-MS spectrometer. The photoionization energy exceeds the computed ionization energies of 8.4-9.0 eV (Table S3) for the four conformers of both MECI and IPCI. Here, we assume that the four conformers of MECI are generated with similar yields, as found in a prior FTMW study,<sup>6</sup> and have similar ionization efficiencies at 10.5 eV. For IPCI, we assume that two conformers, syn2 and anti1, are dominant in Ar carrier gas, as found in a prior FTMW study,<sup>8</sup> and again have similar ionization efficiencies at 10.5 eV. Other isomers may be generated in the source and contribute to the m/z 88 photoionization signals as discussed later, but are not predicted to have strong  $\pi^* \leftarrow \pi$  electronic transitions characteristic of Criegee intermediates.<sup>13</sup>

Resonant excitation of MECI or, alternatively, IPCI results in a UV-induced ground state depletion of one or more of its conformers on its  $\pi^* \leftarrow \pi$  transition. The ground state depletion is readily detected after a short time delay ( $\Delta t \sim 50$  ns) as a reduced VUV photoionization signal detected on the m/z 88 parent mass channel (Figure S4). The integrated photoionization signal (10 Hz) is recorded with and without UV radiation (5 Hz) on alternating laser pulses to obtain to the percentage depletion [(UV<sub>off</sub> – UV<sub>on</sub>) / UV<sub>off</sub>] × 100%. Figure 3 shows the UV-induced depletion as a function of UV power at  $\lambda = 330$  nm, which reaches a maximum of ~79% for MECI and ~57% for IPCI at the highest UV power. For MECI a minimum depletion of 2-3% depletion can be reliably measured, while for IPCI the minimum detectable depletion is ca. 5-6% due to its lower signal level. The extent of depletion can be expressed as ( $N_0 - N/N_0$ ) with  $N_0$  and N representing the ground state abundances before and after UV radiation, respectively. The corresponding absorbance (-ln  $N/N_0$ ) increases linearly with OPO power up to ca. 4 mJ/pulse for both

MECI and IPCI, indicating that the UV absorbance is one-photon process. The large magnitude of the depletions and associated absorbances are indicative of strong electronic transitions for MECI and IPCI, as observed previously for other carbonyl oxide species.<sup>3, 4, 13-16</sup>

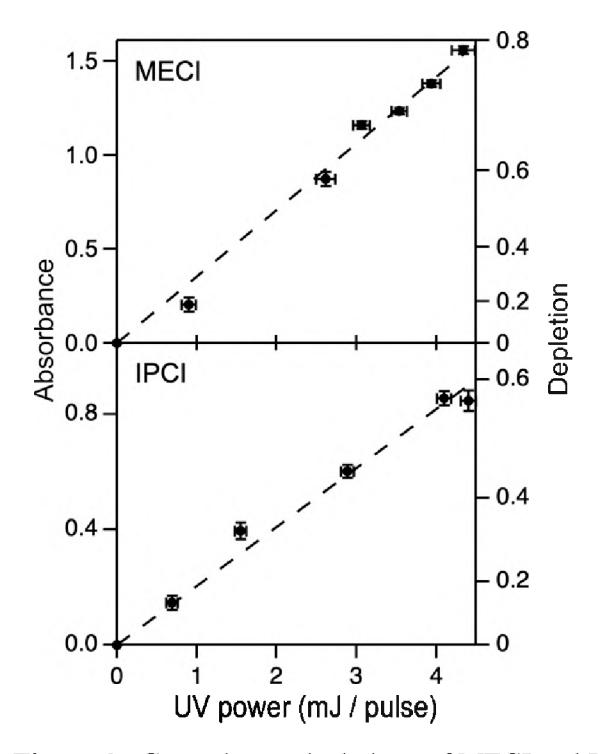


**Figure 3**. Ground state depletions of MECI and IPCI,  $(N_0 - N)/N_0$ , with abundances  $N_0$  before and N after UV irradiation at 330 nm as a function of UV laser power. The corresponding absorbance  $ln(N_0/N)$  change linearly with UV power indicating a one-photon process.

The UV spectra of MECI and IPCI were separately generated by scanning the BBO-OPO across the UV region from 290 to 380 nm in 1 nm steps to obtain their electronic spectra by means of the UV-induced depletion of the associated VUV photoionization signal. Typically, the percentage depletion measured at each UV wavelength is an average of 1500 UV pulses for MECI and 3000 UV pulses for IPCI, respectively. UV-induced depletions were recorded at ca. 2 mJ/pulse for MECI and ca. 3 mJ/pulse for IPCI, measuring UV power at each wavelength, and then normalizing the observed depletions for UV power. The data points are the result of repeated measurements with fit and  $\pm 1\sigma$  uncertainty represented by the solid line and gray shaded region in Figure 4.

The UV spectrum of MECI (10-point smooth) in Figure 4 exhibits a slightly asymmetric shape with a broad peak in the 310 to 330 nm region. The UV spectrum decreases to half-maximum at 300 nm on the shorter wavelength side and 357 nm on the longer wavelength side. IPCI exhibits a bell-shaped UV spectrum that peaks at 330 nm with a full width at half maximum (FWHM) of ca. 40 nm derived from the Gaussian fit (solid line in Figure 4 bottom panel). The IPCI absorbance decreases to half maxima at 303 and 360 nm. In both cases, the minimum absorbance that could be measured by the UV depletion method

occurred at 290 and 380 nm on the shorter and longer wavelength sides, respectively. The peak absorptions of MECI and IPCI are similar to those of other alkyl-substituted Criegee intermediates investigated previously. 15, 16

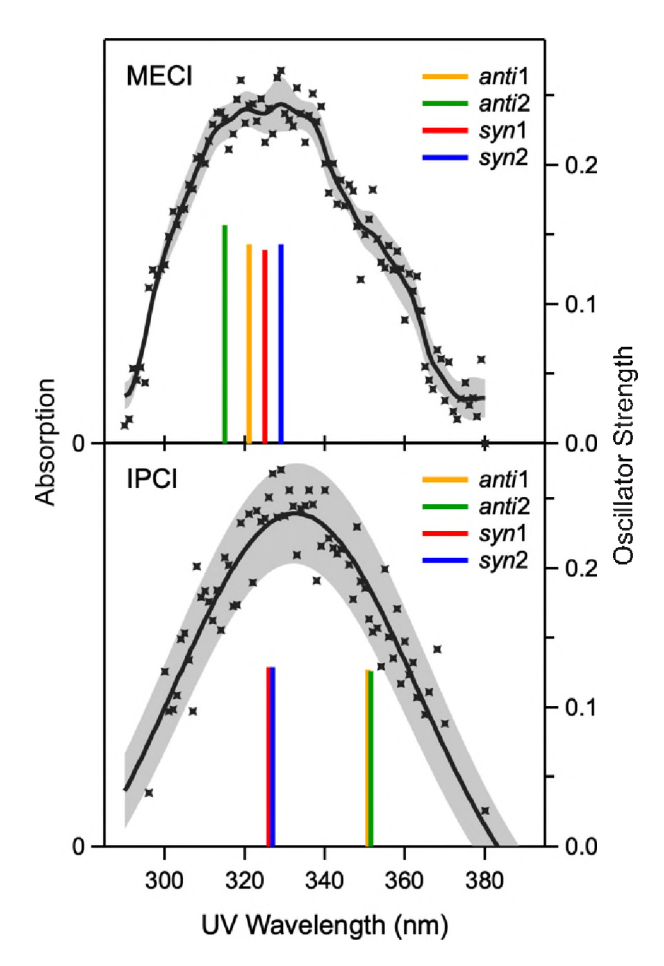


Figure 4. UV absorption spectra of MECI (top) and IPCI (bottom) obtained from the UV-Vis induced depletion method under jet-cooled conditions. Experimental uncertainties from repeated measurements are shown as the gray shaded regions ( $\pm 1\sigma$ ). The solid line (black) through the experimental data represents a smoothed curve (10-point smooth, binomial) for MECI and a Gaussian fit for IPCI. The colored bars indicate the CASPT2(12,10)/AVDZ vertical excitation energies and associated oscillator strengths for promotion from  $S_0$  to the  $S_2$  state for the four conformers in each system.

The vertical excitation energies and corresponding oscillator strengths (f) computed for the optically bright  $S_2 \leftarrow S_0$  transitions of the four conformers of both MECI and IPCI are superimposed on the experimental spectra in Figure 4 and listed in Table 1. The vertical transitions to the strongly absorbing  $S_2$  state with  $\pi\pi^*$  character for the four conformers of MECI are predicted from 315 and 329 nm. By contrast, the analogous transitions in IPCI are grouped together in pairs with the syn and anti conformers at 326 and 351 nm, respectively, with the separation between their electronic transitions arising from intramolecular hydrogen bond stabilization in the ground state and destabilization in the excited state of

syn conformers.<sup>15</sup> The predominant orbitals contributing to the  $\pi^* \leftarrow \pi$  transitions, shown in Figure S5, are mainly associated with electronic promotion from the HOMO-1 ( $\pi$ ) orbital to the LUMO ( $\pi^*$ ) orbital, the latter of which shows increased antibonding character around the carbonyl oxide moiety. By contrast, the S<sub>1</sub>  $\leftarrow$  S<sub>0</sub> transitions are predicted to be weak with negligible oscillator strength. The experimental spectra for MECI and IPCI are in good accord with the theoretically predicted VEE associated with transitions to the S<sub>2</sub> state with  $\pi\pi^*$  character. The experimental spectra span broad range of 40-60 nm (FWHM) reflecting the overlapping transitions associated with the four conformers of MECI and at least two conformers of IPCI, along with Franck-Condon overlap to the excited  $\pi\pi^*$  electronic state.

**Table 1**. Vertical excitation energies (VEE, eV), corresponding wavelengths ( $\lambda$ , nm), and oscillator strengths (f) computed at the SA5-CASPT2(12,10)/aug-cc-pVDZ level of theory for electronic transitions of the four conformers of MECI and IPCI to the  $^1\pi\pi^*$  state.

Criegee intermediate	conformer	VEE [eV] (λ [nm])	f
MECI	anti l	3.86 (321)	0.143
	anti2	3.93 (315)	0.157
	syn1	3.81 (325)	0.139
	syn2	3.76 (329)	0.143
IPCI	anti l	3.54 (351)	0.127
	anti2	3.53 (351)	0.126
	syn1	3.81 (326)	0.129
	syn2	3.80 (327)	0.129

We anticipate that the  $\pi\pi^*$  states of MECI and IPCI are dissociative in nature at the energies accessed by vertical excitation from their respective ground states. As shown in prior theoretical studies of Criegee intermediates, <sup>13</sup> the first excited  $^1\pi\pi^*$  state couples via conical intersections to various electronic states that are repulsive with respect to O-O bond elongation and lead to the lowest spin-allowed dissociation asymptote. The lowest spin-allowed dissociation asymptote from *anti*1-MECI to O ( $^1$ D) + butanone [CH<sub>3</sub>C(O)CH<sub>2</sub>CH<sub>3</sub>, X  $^1$ A'] products is predicted at 2.16 eV, while for *syn*2-IPCI to O ( $^1$ D) + isopropylaldehyde [(CH<sub>3</sub>)<sub>2</sub>CHCHO, X  $^1$ A] the product asymptote is computed at 2.37 eV (see Table S4). In both cases, the asymptotic limits are far lower than the UV excitation energies, suggesting prompt O-O bond fission following  $\pi\pi^*$  excitation as found for CH<sub>2</sub>OO and other alkyl-substituted Criegee intermediates. <sup>17-21</sup>

The absorption cross sections for MECI and IPCI are estimated by comparing their measured absorbances (Figure 4) with that obtained for CH<sub>2</sub>OO under the same experimental conditions in this laboratory, in particular with the same OPO beam profile and focusing conditions. The power normalized absorbance of CH<sub>2</sub>OO obtained at 308, 330, 340, and 355 nm (Table S5) is then scaled to the average of

the cross section reported for CH<sub>2</sub>OO at its 340 nm peak  $[1.2 \pm 0.2 \times 10^{-17} \text{ cm}^2]$  by Ting et al.<sup>22</sup> This comparison yields peak absorption cross sections for MECI and IPCI at 330 nm that are slightly larger (at most 50% larger) than CH<sub>2</sub>OO, but still on the order of  $10^{-17} \text{ cm}^2$ . The cross sections for MECI and IPCI are similar to those derived for previously studied Criegee intermediates, including CH<sub>2</sub>OO,<sup>14, 22</sup> CH<sub>3</sub>CHOO,<sup>15, 23</sup> (CH<sub>3</sub>)<sub>2</sub>COO,<sup>16, 24</sup> CH<sub>3</sub>CH<sub>2</sub>COO.<sup>16</sup> However, it is important to note that the MECI spectrum has contributions from four conformers and the IPCI spectrum has components from at least two conformers, which is not taken into account in the estimated UV absorbances.

There are many possible isomers of MECI and IPCI (m/z 88) that may be ionized at 10.5 eV (Table S6). However, we have not identified a plausible isomer that is also predicted to have strong electronic transitions in the 300-500 nm region. Nevertheless, we have computed vertical excitation energies and oscillator strengths for possible isomers of MECI and IPCI in Table S6. These isomers may result from unimolecular decay via 1,4 H-atom transfer to form vinyl hydroperoxides,  $^{25,26}$  or subsequent OH roaming to the vinyl moiety, forming  $\alpha$ -hydroxy carbonyl compounds. Other possibilities include esters or carboxylic acid products that might arise from 1,3 ring closure of the Criegee intermediates to form dioxiranes and subsequent products. Any of these isomers, if formed, could contribute to residual 10.5 eV photoionization signal (m/z 88), which is not depleted by the UV laser on the strong  $\pi^* \leftarrow \pi$  transitions investigated herein.

Finally, we return to our primary goal of comparing the electronic spectra of MECI and IPCI with those previously obtained for MVK-oxide and MACR-oxide, respectively. The four CI have similar backbone connectivity (see Scheme 1), but the latter two isoprene-derived CI differ in having extended conjugation across the vinyl and carbonyl oxide groups. MVK-oxide and MACR-oxide have two distinct excited singlet  $\pi\pi^*$  states that are optically bright.<sup>3, 4</sup> Here, we focus on their first  $\pi\pi^*$  excited states with  $\pi^*$  character on the C=O<sup>+</sup>O<sup>-</sup> moiety, which are analogous to the optically bright  $\pi\pi^*$  states of MECI and IPCI. Comparison of the molecular orbitals associated with the  $\pi^*\leftarrow\pi$  transitions of selected conformers of MECI and IPCI with MVK-oxide and MACR-oxide are shown in Figure S6. The four conformers of MECI are predicted to have VEE between 315 and 329 nm, while for MVK-oxide the vertical excitation to the 1  $^1\pi\pi^*$  state occurs between 350 and 392 nm.<sup>3</sup> Similarly, the two distinct conformers of IPCI are predicted to have VEE at 326 and 351 nm, while the four conformers of MACR-oxide have VEE to the  $1^1\pi\pi^*$  state between 342 and 380 nm.<sup>4</sup> In both cases, the significant red shift predicted for the electronic transition of the unsaturated substituted Criegee intermediates is due to extended conjugation of  $\pi$  orbitals across the C=C and C=O<sup>+</sup>O<sup>-</sup> groups, which leads to a decrease in the energy gap between the HOMO-1 (or HOMO in MACR-oxide) and LUMO orbitals.

MVK-oxide and MACR-oxide both have more extended  $\pi$ -conjugation than MECI and IPCI, and their corresponding  $\pi^* \leftarrow \pi$  absorptions occur at significantly longer wavelengths than those of MECI and IPCI recorded under similar experimental conditions.<sup>3,4</sup> As shown in Figure 5, both MVK-oxide and MACR-oxide display broad absorption spectra with peak absorption at 388 and 380 nm, respectively, and extend into the visible region where the solar actinic flux penetrating the atmosphere is rapidly increasing. The onset of another absorption band is evident in the spectra of MVK-oxide and MACR-oxide at  $\lambda$  < 300 and 350 nm, respectively.<sup>4,29</sup> This is consistent with excitation to a second  $^1\pi\pi^*$  excited state in which the dominant participating orbitals are more localized on the C=C moiety. The peak absorptions of MVK-oxide and MACR-oxide to the first  $^1\pi\pi^*$  excited state are both shifted a remarkable 50 nm to longer wavelength than those reported here for MECI and IPCI at 320 and 330 nm, respectively, reflecting the extended conjugation in the resonance-stabilized systems.

The electronic spectra of MVK-oxide and MACR-oxide on the first  $\pi^* \leftarrow \pi$  transition have also been reported by direct absorption methods under thermal conditions.<sup>30, 31</sup> The spectra obtained by the two methods peak at similar wavelengths, but there are also notable differences. The variations may be due to the different temperatures ( $T_{rot} \sim 10 \text{ K vs. } T \sim 300 \text{ K}$ ) and/or the timescales for the experimental measurements, which is on the order of microseconds for the jet-cooled studies compared with, typically, milliseconds for the thermal absorption measurements. The latter may allow rapid unimolecular decay processes to deplete population of specific conformers of MVK-oxide and MACR-oxide, such as those that decay by rapid ring closure to dioxole (2140 s<sup>-1</sup> and 2500 s<sup>-1</sup>, respectively, at 298 K and 760 Torr).<sup>2, 5, 32</sup> The most recent direct absorption study also yielded absorption cross sections for MVK-oxide and MACR-oxide that are larger than  $CH_2OO$  and simpler, alkyl-substituted  $CIs [syn-CH_3CHOO, (CH<sub>3</sub>)<sub>2</sub>COO]$ , consistent with extended conjugation in the isoprene-derived CI.<sup>31</sup>

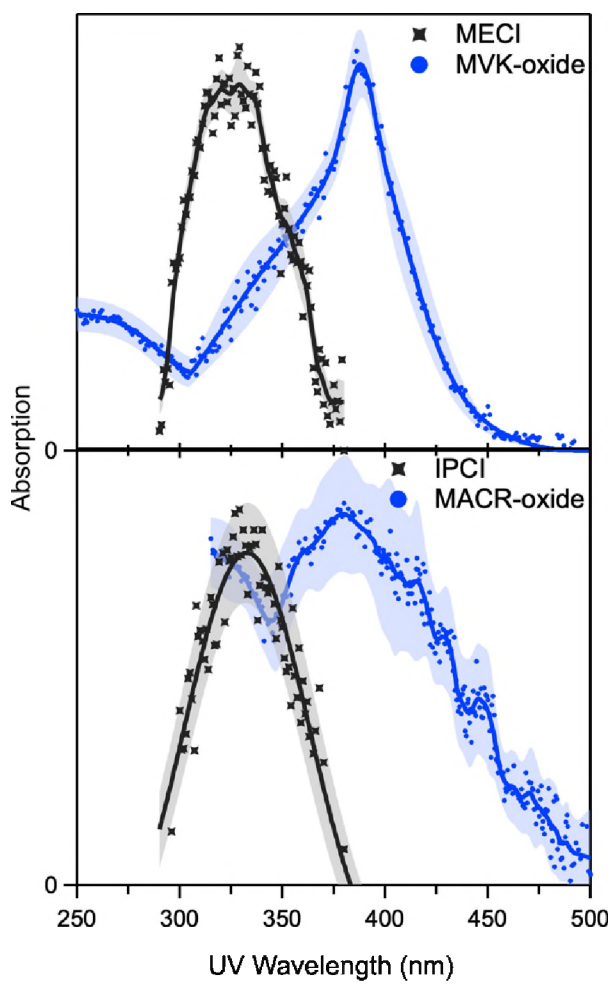


Figure 5. Comparison of UV-vis absorption spectra obtained for MECI with MVK-oxide (top) and IPCI with MACR-oxide (bottom) under jet-cooled conditions. The vinyl-substituted CIs (blue) formed in isoprene ozonolysis have peak absorptions shifted ca. 50 nm to longer wavelength than analogous alkyl-substituted CIs (black). Note that the increase in absorption at shorter wavelengths in the blue traces arises from the second  $\pi^* \leftarrow \pi$  transition associated with the vinyl group. The MVK-oxide spectrum is reproduced from J. Chem. Phys. 155, 174305 (2021) with the permission of AIP Publishing.<sup>29</sup> The MACR-oxide spectrum is reproduced from J. Am. Chem. Soc. 141, 15058-15069 (2019).<sup>4</sup>

## **Conclusions**

Four-carbon Criegee intermediates with methyl-ethyl and isopropyl substituents, MECI and IPCI, respectively, have been separately characterized on the strong  $\pi^* \leftarrow \pi$  electronic transition associated with the carbonyl oxide group. Their electronic spectra have each been recorded by UV-induced depletion of the associated VUV (10.5 eV) photoionization signal at m/z 88. The strong UV-induced depletion, attributed to one or more of the four conformers of MECI or IPCI, is peaked at 320 or 330 nm, respectively, in a linear absorption process. The broad and unstructured electronic spectra for MECI and IPCI span from 300 to 357 nm and 303 to 360 nm (FWHM), respectively, with peak absorption cross

sections on the order of  $10^{-17}$  cm<sup>2</sup> ascertained by comparison with the well-characterized absorption of CH<sub>2</sub>OO recorded under similar experimental conditions.<sup>22</sup> Complementary theoretical calculations predict vertical transition energies and large oscillator strengths for transitions to the  $\pi\pi^*$  states of the four conformers of MECI in the 315 to 329 nm region and as pairs of transitions for the two *syn*- and two *anti*-conformers of IPCI at 326 and 351 nm, respectively. The latter are more separated due to intramolecular hydrogen-bonding in *syn*-conformers of IPCI. The UV absorptions of MECI and IPCI promote the four-carbon Criegee intermediates to energies significantly above their spin-allowed dissociative asymptotes, which lead to O ( $^{1}$ D) + butanone or isopropylaldehyde products.

Comparison of the electronic spectra of the four-carbon Criegee intermediates with alkyl substituents investigated here with prior studies of MVK-oxide<sup>3, 30</sup> and MACR-oxide<sup>4, 33</sup> with unsaturated substituents reveals significant changes for systems with similar structures and backbone connectivity. The first  $\pi^* \leftarrow \pi$  transitions of MVK-oxide and MACR-oxide are shifted a remarkable 50 nm to longer wavelength than those for MECI and IPCI, respectively, reflecting the extended  $\pi$  conjugation across the carbonyl oxide and vinyl groups in the isoprene-derived Criegee intermediates. Changes are also evident in the unimolecular and bimolecular reaction pathways accessible in MVK-oxide and MACR-oxide<sup>2, 30, 32-34</sup> compared to CH<sub>2</sub>OO or alkyl-substituted CI systems.<sup>35</sup> Further studies are needed to examine the properties of CI derived from ozonolysis of more complicated biogenic alkenes, such as  $\alpha$ -pinene or other terpenes, where conjugation, carbon chain length and steric hindrance may play a role.

## **Supporting Information Description**

Supporting information details precursor synthesis and experimental and computed properties of the four-carbon Criegee intermediates, including conformer, ionization, dissociation, and electronic energies.

#### Acknowledgements

This research is supported through the U.S. Department of Energy Basic Energy Sciences under Grant No. DE-FG02-87ER13792. This work utilized the Extreme Science and Engineering Discovery Environment (XSEDE), which is supported by the National Science Foundation grant number ACI-1548562 through the allocation TG-CHE190088. CAS thanks the National Science Foundation under grant CHE-2102626 (to Marisa Kozlowski, PI) for support. The authors thank Tolga Karsili (University of Louisiana) for helpful discussions on CASPT2 calculations.

<sup>†</sup> T.L. and M.Z. contributed equally to this paper.

<sup>‡</sup> Present address: Aerospace Mechanics Research Center, University of Colorado, Boulder, CO 80303 USA

#### References

- (1) Sindelarova, K.; Granier, C.; Bouarar, I.; Guenther, A.; Tilmes, S.; Stavrakou, T.; Muller, J. F.; Kuhn, U.; Stefani, P.; Knorr, W. Global data set of biogenic VOC emissions calculated by the MEGAN model over the last 30 years. *Atmos. Chem. Phys.* **2014**, *14* (17), 9317-9341. **DOI**: 10.5194/acp-14-9317-2014.
- (2) Barber, V. P.; Pandit, S.; Green, A. M.; Trongsiriwat, N.; Walsh, P. J.; Klippenstein, S. J.; Lester, M. I. Four-Carbon Criegee Intermediate from Isoprene Ozonolysis: Methyl vinyl ketone oxide synthesis, infrared spectrum, and OH production. *J. Am. Chem. Soc.* **2018**, *140* (34), 10866-10880. DOI: 10.1021/jacs.8b06010.
- (3) Vansco, M. F.; Marchetti, B.; Lester, M. I. Electronic spectroscopy of methyl vinyl ketone oxide: A four-carbon unsaturated Criegee intermediate from isoprene ozonolysis. *J. Chem. Phys.* **2018**, *149* (24). **DOI**: 10.1063/1.5064716.
- (4) Vansco, M. F.; Marchetti, B.; Trongsiriwat, N.; Bhagde, T.; Wang, G. H.; Walsh, P. J.; Klippenstein, S. J.; Lester, M. I. Synthesis, electronic spectroscopy, and photochemistry of methacrolein oxide: a four-carbon unsaturated Criegee intermediate from isoprene ozonolysis. *J. Am. Chem. Soc.* **2019**, *141* (38), 15058-15069. DOI: 10.1021/jacs.9b05193.
- (5) Vereecken, L.; Novelli, A.; Taraborrelli, D. Unimolecular decay strongly limits the atmospheric impact of Criegee intermediates. *Phys. Chem. Chem. Phys.* **2017**, *19* (47), 31599-31612. **DOI**: 10.1039/c7cp05541b.
- (6) Cabezas, C.; Guillemin, J.-C.; Endo, Y. Probing the conformational behavior of the doubly substituted methyl-ethyl Criegee intermediate by FTMW spectroscopy. *J. Chem. Phys.* **2017**, *146* (17), 174304. DOI: 10.1063/1.4982682.
- (7) Barber, V. P.; Hansen, A. S.; Georgievskii, Y.; Klippenstein, S. J.; Lester, M. I. Experimental and theoretical studies of the doubly substituted methyl-ethyl Criegee intermediate: Infrared action spectroscopy and unimolecular decay to OH radical products. *J. Chem. Phys.* **2020**, *152* (9). DOI: 10.1063/5.0002422.
- (8) Cabezas, C.; Guillemin, J. C.; Endo, Y. Conformational preferences of Criegee intermediates: Isopropyl substituted carbonyl oxide. *J. Chem. Phys.* **2018**, *149* (8). **DOI**: 10.1063/1.5045768.
- (9) Frisch, M. J.; Trucks, G. W.; Schlegel, H. B.; Scuseria, G. E.; Robb, M. A.; Cheeseman, J. R.; Scalmani, G.; Barone, V.; Petersson, G. A.; Nakatsuji, H., et al. *Gaussian 16* Rev. C.01; Gaussian, Inc.: Wallingford, CT, 2016.
- (10) Werner, H. J.; Knowles, P. J.; Knizia, G.; Manby, F. R.; Schutz, M. Molpro: a general-purpose quantum chemistry program package. *Wiley Interdiscip. Rev. Comput. Mol. Sci.* **2012**, *2* (2), 242-253. DOI: 10.1002/wcms.82.
- (11) Werner, H. J.; Knowles, P. J.; Manby, F. R.; Black, J. A.; Doll, K.; Hesselmann, A.; Kats, D.; Kohn, A.; Korona, T.; Kreplin, D. A., et al. The Molpro quantum chemistry package. *J. Chem. Phys.* **2020**, *152* (14). DOI: 10.1063/5.0005081.

- (12) Werner, H. J.; Knowles, P. J.; Knizia, G.; Manby, F. R.; Schutz, M.; Celani, W.; Gyorffy, D.; Kats, T.; Korona, R.; Lindh, A., et al. *MOLPRO*, 2020, a package of ab initio programs; 2020. https://www.molpro.net
- (13) Karsili, T. N. V.; Marchetti, B.; Lester, M. I.; Ashfold, M. N. R. Electronic absorption spectroscopy and photochemistry of Criegee intermediates. *Photochem. Photobiol.* **2022**. DOI: 10.1111/php.13665.
- (14) Beames, J. M.; Liu, F.; Lu, L.; Lester, M. I. Ultraviolet spectrum and photochemistry of the simplest Criegee intermediate CH<sub>2</sub>OO. *J. Am. Chem. Soc.* **2012**, *134* (49), 20045-20048. DOI: 10.1021/ja310603j.
- (15) Beames, J. M.; Liu, F.; Lu, L.; Lester, M. I. UV spectroscopic characterization of an alkyl substituted Criegee intermediate CH<sub>3</sub>CHOO. *J. Chem. Phys.* **2013**, *138* (24). DOI: 10.1063/1.4810865.
- (16) Liu, F.; Beames, J. M.; Green, A. M.; Lester, M. I. UV Spectroscopic characterization of dimethyland ethyl-substituted carbonyl oxides. *J. Phys. Chem. A* **2014**, *118* (12), 2298-2306. DOI: 10.1021/jp412726z.
- (17) Esposito, V. J.; Liu, T.; Wang, G.; Caracciolo, A.; Vansco, M. F.; Marchetti, B.; Karsili, T. N. V.; Lester, M. I. Photodissociation dynamics of CH<sub>2</sub>OO on multiple potential energy surfaces: experiment and theory. *J. Phys. Chem. A* **2021**, *125* (30), 6571-6579. DOI: 10.1021/acs.jpca.1c03643.
- (18) Lehman, J. H.; Li, H. W.; Beames, J. M.; Lester, M. I. Communication: Ultraviolet photodissociation dynamics of the simplest Criegee intermediate CH<sub>2</sub>OO. *J. Chem. Phys.* **2013**, *139* (14). DOI: 10.1063/1.4824655.
- (19) Li, H. W.; Fang, Y.; Beames, J. M.; Lester, M. I. Velocity map imaging of O-atom products from UV photodissociation of the CH<sub>2</sub>OO Criegee intermediate. *J. Chem. Phys.* **2015**, *142* (21). DOI: 10.1063/1.4921990.
- (20) Li, H. W.; Fang, Y.; Kidwell, N. M.; Beames, J. M.; Lester, M. I. UV Photodissociation dynamics of the CH<sub>3</sub>CHOO Criegee intermediate: action spectroscopy and velocity map imaging of O-atom products. *J. Phys. Chem. A* **2015**, *119* (30), 8328-8337. DOI: 10.1021/acs.jpca.5b05352.
- (21) Vansco, M. F.; Li, H. W.; Lester, M. I. Prompt release of O <sup>1</sup>D products upon UV excitation of CH<sub>2</sub>OO Criegee intermediates. *J. Chem. Phys.* **2017**, *147* (1). DOI: 10.1063/1.4977987.
- (22) Ting, W. L.; Chen, Y. H.; Chao, W.; Smith, M. C.; Lin, J. J. M. The UV absorption spectrum of the simplest Criegee intermediate CH<sub>2</sub>OO. *Phys. Chem. Chem. Phys.* **2014**, *16* (22), 10438-10443. DOI: 10.1039/c4cp00877d.
- (23) Smith, M. C.; Ting, W. L.; Chang, C. H.; Takahashi, K.; Boering, K. A.; Lin, J. J. M. UV absorption spectrum of the C2 Criegee intermediate CH<sub>3</sub>CHOO. *J. Chem. Phys.* **2014**, *141* (7). DOI: 10.1063/1.4892582.
- (24) Chang, Y. P.; Chang, C. H.; Takahashi, K.; Lin, J. J. M. Absolute UV absorption cross sections of dimethyl substituted Criegee intermediate (CH<sub>3</sub>)<sub>2</sub>COO. *Chem. Phys. Lett.* **2016**, *653*, 155-160. **DOI**: 10.1016/j.cplett.2016.04.082.
- (25) Lester, M. I.; Klippenstein, S. J. Unimolecular decay of Criegee intermediates to OH radical products: prompt and thermal decay processes. *Acc. Chem. Res.* **2018**, *51* (4), 978-985. DOI: 10.1021/acs.accounts.8b00077.

- (26) Stephenson, T. A.; Lester, M. I. Unimolecular decay dynamics of Criegee intermediates: Energy-resolved rates, thermal rates, and their atmospheric impact. *Int. Rev. Phys. Chem.* **2020**, *39* (1), 1-33. DOI: 10.1080/0144235X.2020.1688530.
- (27) Taatjes, C. A.; Liu, F.; Rotavera, B.; Kumar, M.; Caravan, R.; Osborn, D. L.; Thompson, W. H.; Lester, M. I. Hydroxyacetone Production From C<sub>3</sub> Criegee Intermediates. *J. Phys. Chem. A* **2017**, *121* (1), 16-23. DOI: 10.1021/acs.jpca.6b07712.
- (28) Liu, T.; Zou, M.; Vansco, M. F.; Markus, C. R.; Almeida, R.; Au, K.; Sheps, L.; Osborn, D. L.; Percival, C. J.; Taatjes, C. A., et al. *manuscript in preparation*.
- (29) Wang, G.; Liu, T.; Caracciolo, A.; Vansco, M. F.; Trongsiriwat, N.; Walsh, P. J.; Marchetti, B.; Karsili, T. N. V.; Lester, M. I. Photodissociation dynamics of methyl vinyl ketone oxide: A four-carbon unsaturated Criegee intermediate from isoprene ozonolysis. *J. Chem. Phys.* **2021**, *155* (17), 174305. DOI: 10.1063/5.0068664.
- (30) Caravan, R. L.; Vansco, M. F.; Au, K.; Khan, M. A. H.; Li, Y. L.; Winiberg, F. A. F.; Zuraski, K.; Lin, Y. H.; Chao, W.; Trongsiriwat, N., et al. Direct kinetic measurements and theoretical predictions of an isoprene-derived Criegee intermediate. *Proc. Natl. Acad. Sci. U.S.A.* **2020**, *117* (18), 9733-9740. DOI: 10.1073/pnas.1916711117.
- (31) Lin, Y. H.; Takahashi, K.; Lin, J. J. M. Absolute photodissociation cross sections of thermalized methyl vinyl ketone oxide and methacrolein oxide. *Phys. Chem. Chem. Phys.* **2022**, *24* (17), 10439-10450. **DOI**: 10.1039/d2cp00476c.
- (32) Vansco, M. F.; Caravan, R. L.; Zuraski, K.; Winiberg, F. A. F.; Au, K.; Trongsiriwat, N.; Walsh, P. J.; Osborn, D. L.; Percival, C. J.; Khan, M. A. H., et al. Experimental evidence of dioxole unimolecular decay pathway for isoprene-derived Criegee intermediates. *J. Phys. Chem. A* **2020**, *124* (18), 3542-3554. DOI: 10.1021/acs.jpca.0c02138.
- (33) Lin, Y. H.; Yin, C.; Takahashi, K.; Lin, J. M. Surprisingly long lifetime of methacrolein oxide, an isoprene derived Criegee intermediate, under humid conditions. *Commun. Chem.* **2021**, *4* (1). DOI: 10.1038/s42004-021-00451-z.
- (34) Lin, Y. H.; Yang, C. H.; Takahashi, K.; Lin, J. J. M. Kinetics of unimolecular decay of methyl vinyl ketone oxide, an isoprene-derived Criegee intermediate, under atmospherically relevant conditions. *J. Phys. Chem. A* **2020**, *124* (45), 9375-9381. DOI: 10.1021/acs.jpca.0c07928.
- (35) Caravan, R. L.; Vansco, M. F.; Lester, M. I. Open questions on the reactivity of Criegee intermediates. *Commun. Chem.* **2021**, *4* (1). DOI: 10.1038/s42004-021-00483-5.

TOC Graphic

